

A NUMERICAL SIMULATION METHOD FOR CALCULATION OF LINEAR ATTENUATION COEFFICIENTS OF UNIDENTIFIED SAMPLE MATERIALS IN ROUTINE GAMMA RAY SPECTROMETRY

by

Mohamed S. BADAWI

Physics Department, Faculty of Science, Alexandria University, Alexandria, Egypt

Scientific paper
DOI: 10.2298/NTRP1504249B

When using gamma ray spectrometry for radioactivity analysis of environmental samples (such as soil, sediment or ash of a living organism), relevant linear attenuation coefficients should be known – in order to calculate self-absorption in the sample bulk. This parameter is additionally important since the unidentified samples are normally different in composition and density from the reference ones (the latter being *e. g.* liquid sources, commonly used for detection efficiency calibration in radioactivity monitoring). This work aims at introducing a numerical simulation method for calculation of linear attenuation coefficients without the use of a collimator. The method is primarily based on calculations of the effective solid angles – compound parameters accounting for the emission and detection probabilities, as well as for the source-to-detector geometrical configuration. The efficiency transfer principle and average path lengths through the samples themselves are employed, too. The results obtained are compared with those from the NIST-XCOM data base; close agreement confirms the validity of the numerical simulation method approach.

Key words: gamma ray spectrometry, linear attenuation coefficient, effective solid angle, path length, numerical simulation method

INTRODUCTION

Gamma ray spectrometry is one of the most widely used techniques for determining the concentration of natural and artificial radionuclides in environmental samples. Germanium detectors with high gamma ray resolution were used to allow a precise quantitative determination of the radioactive concentration of the samples [1]. Being a non-destructive multi-element analysis, its major advantage is that there is almost no need for any kind of a chemical separation process and its suitability to all sample types [2].

Normally, environmental radioactivity samples are different in their composition from the calibration sources. Most of the standard radioactive volumetric sources are made by considering the geometry configuration of the samples. It is hard to neglect the difference in the sample's composition such as soil, sediment and the ash of living organisms, because their densities are different. The difference in the self-attenuation of gamma rays in sample materials should be considered in the calculation of detector full-energy peak efficiency and in the environmental analysis pro-

cess. Self-attenuation is caused by the absorption and scattering of the gamma rays in the sample matrix itself, and leads to inaccurate measurement of radioactivity with large percentages, particularly for samples emitting low-energy gamma rays [3-5]. Correcting detection efficiency for the self-attenuation effect makes a more accurate analysis achievable; consequently, the correction of the difference in self-attenuation between the volumetric sources and the environmental samples is required in gamma ray spectrometry.

The linear attenuation coefficient is considered to be the crucial correction factor in self-attenuation estimation. The attenuation of gamma rays through composite materials is of interest for industrial, medical and agricultural studies and in many other fields. Its properties suite a wide range of elements and composite materials from the National Institute for Standards and Technology NIST-XCOM database. The linear attenuation coefficient mainly depends on photon energy and the nature of the samples such as chemical composition and density [6-12]. In addition, for most environmental analyses, the value of the linear attenuation coefficient is not known and should be estimated by measurement or use of samples of assumed composition and density. The distribution of path

* Corresponding author; e-mail: ms241178@hotmail.com

lengths via samples of photons contributing to the peak count rate depends on sample geometry and, slightly less, on detector dimensions and photon energy [13, 14].

This work introduces a novel and accurate numerical simulation method (NSM) for calculating the linear attenuation coefficient by use of analytical modeling of source-to-detector configurations and numerical integration solutions. In it, axially isotropic radiating gamma ray point sources are used to create a photon cone-beam without the use of a collimator. Plexiglass vials with diameters smaller than the diameter of the crystal detector were filled with reference sample materials [NaCl, Na₂CO₃, and (NH₄)₂SO₄] similar to the densities of the environmental samples. In the study, a new NSM method was used to calculate the linear attenuation coefficient of the samples. The integrations were solved numerically, via the trapezoidal rule. The accuracy of the integration increases with an increase in the number of intervals n, the integration value converging well at n = 20.

The methodology applied is as follows. *Mathematical model* of this study presents, in detail, the analytical calculation of the effective solid angle and linear attenuation coefficient using samples of various shapes and dimensions. *Experimental materials and methods* includes the experimental work with materials and methods. *Results and discussion* contains the comparisons between the calculated linear attenuation coefficient via the recent approach and the NIST-XCOM data showing the validity of the current approach. Our conclusions are presented in *Conclusion*.

MATHEMATICAL MODEL

When the gamma rays emitted from an isotropic radiating point source pass through the sample mate-

rial, they undergo attenuation primarily through incoherent Compton scattering and photoelectric and pair production interactions [15]. As shown in figs. 1 and 2, the attenuation of gamma rays as they pass through matter are relevant for a number of fields, such as shielding radiation sources and tumor irradiation, to mention but a few. The mathematical expression, showing an exponential decrease of gamma ray intensity with material thickness (*i. e.* photon path-length through the material), is given

$$I = I_0 e^{-\mu x} \tag{1}$$

Considering that: I_0 is the original gamma ray intensity I is the gamma-ray intensity transmitted through the sample of thickness x , while μ is the linear attenuation coefficient of that sample. This attenuation is found to be strongly dependent on the density of the sample material, where more atoms and heavier atoms in the way of the photons mean more interactions per unit length of the sample. Therefore, the linear attenuation coefficient will have different values for the same material, depending on its phase (solid, liquid or vapor) and its temperature [15]. For this reason, it's convenient to define a mass attenuation coefficient μ_m , as

$$\mu_m = \frac{\mu}{\rho} \tag{2}$$

where ρ is the sample density.

This quantity is independent of density and, hence, it is the same for the sample, regardless of its phase and temperature and approximately independent of the type of sample, as well. In addition, the linear attenuation coefficient μ , can also be written as the sum over contributions from the principle photon interactions [15] and can be given as

$$\mu = \mu_{PE} + \mu_{INCOH} + \mu_{PP} \tag{3}$$

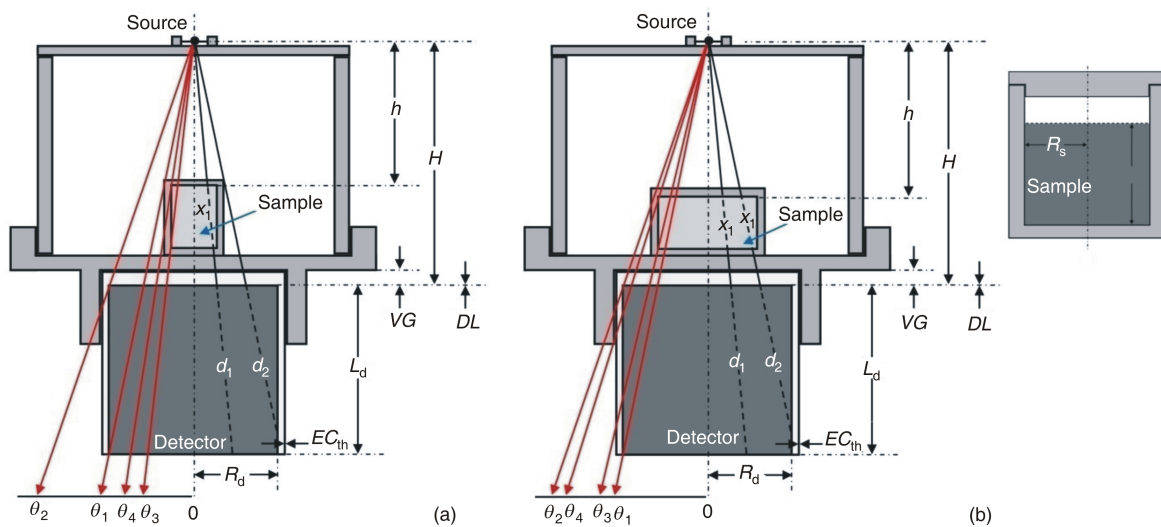


Figure 1. The geometry of the sample in arrangement between source-to-detector; (a) in case $\theta_2 > \theta_1 > \theta_4 > \theta_3$, (b) in case $\theta_2 > \theta_4 > \theta_3 > \theta_1$

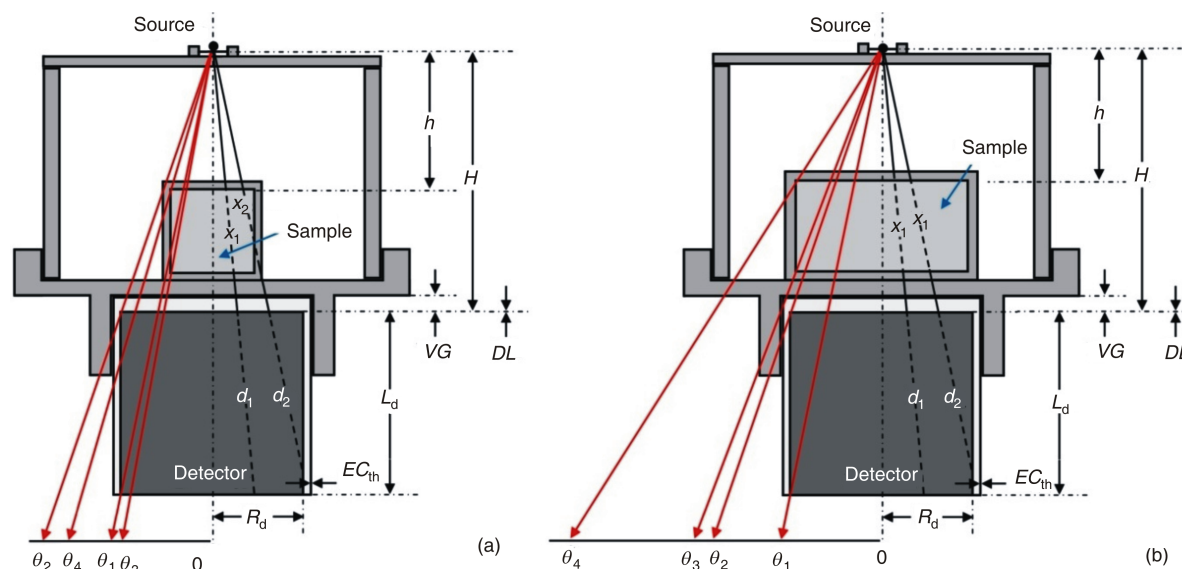


Figure 2. The geometry of the sample in arrangement between source-to-detector; (a) in case $\theta_2 > \theta_4 > \theta_1 > \theta_3$ (b) in case $\theta_4 > \theta_3 > \theta_2 > \theta_1$

where μ_{PE} , μ_{INCOH} , and μ_{PP} , are the photoelectric, Compton, and pair production coefficients, respectively, corresponding to the energy of the incident photon. The theoretical linear and mass attenuation coefficients can be estimated by using NIST-XCOM software. XCOM software can produce cross sections on a standard energy grid, selected by the user, or for a mix of both grids, at energies between 1 keV and 100 GeV. This software uses the mixing rule to calculate the partial and total mass attenuation coefficients for all elements, compounds and mixtures at standard and selected energies.

In order to calculate the linear attenuation coefficient of any sample material, a new numerical simulation method (NSM) based on the direct method and an efficiency transfer method [16-19] will be applied in terms of the gamma-ray count rate and detector efficiency given as

$$\frac{N}{N_0} \bigg|_{measured} = \frac{\varepsilon}{\varepsilon_0} \bigg|_{measured} \frac{\varepsilon_2}{\varepsilon_1} \bigg|_{calculated} \frac{\Omega_{Eff2}}{\Omega_{Eff1}} S_f \quad (4)$$

N and N_0 , are the measured count rates of gamma rays using the vial filled with sample material and an empty vial, respectively. This can be done by using an isotropic radiating axial point source located at a certain distance from the vial, positioned on the detector surface. Also, ε , and ε_0 , are the measured efficiencies of the detector determined under the same conditions as the count rates [18, 19]. The measured full-energy peak efficiency of a photon at energy E , can be determined by using the equation

$$\varepsilon(E) = \frac{N(E)}{TA_S P(E)} C_i \quad (5)$$

where $N(E)$ is the number of counts in the full-energy peak, T – the measuring time (in seconds), $P(E)$ – the photon emission probability at energy E , A_S – the radionuclide activity, and C_i , the correction factors due to radionuclide half-life. The decay correction C_d , for the calibration source from the reference time to the run time is given by

$$C_d = e^{\lambda \Delta T} \quad (6)$$

where λ is the decay constant and T – the time interval from the reference time in which the source decays corresponding to the run time. The uncertainty in the experimental full-energy peak efficiency, σ_ε is given by

$$\sigma_\varepsilon = \varepsilon \sqrt{\left(\frac{\partial \varepsilon}{\partial A}\right)^2 \sigma_A^2 + \left(\frac{\partial \varepsilon}{\partial P}\right)^2 \sigma_P^2 + \left(\frac{\partial \varepsilon}{\partial N}\right)^2 \sigma_N^2} \quad (7)$$

where σ_A , σ_P , and σ_N are the uncertainties associated with the quantities A_S , $P(E)$, and $N(E)$, respectively [18, 19].

In addition, ε_2 and ε_1 , are the calculated detection efficiencies under the same conditions [18]. This calculated full-energy peak efficiency can be calculated by using the equation

$$\varepsilon_1 = \varepsilon^* \frac{\Omega_{Eff1}}{\Omega^*} \text{ and } \varepsilon_2 = \varepsilon^* \frac{\Omega_{Eff2}}{\Omega^*} \quad (8)$$

where ε^* and Ω^* are the measured reference full-energy peak efficiencies of the detector and effective solid angles subtended by the source-to-detector. In our configuration, this can be done by using an isotropic radiating axial point located at any distance from the detector surface in the absence of the vial. Also, Ω_{Eff2} , and Ω_{Eff1} , are the effective solid angles subtended by the detector surface in the presented vial

filled with sample material and an empty vial, respectively, under the same conditions as the count rates.

In case of the volumetric sample presented, not all of the emitted photons leave the sample; some are absorbed by the sample itself, effecting efficiency calculations. The factor concerning this effect is called the self-absorption factor S_f , given as in eq. (4) by

$$S_f = e^{-\mu_s \bar{x}_s} \tag{9}$$

where μ_s is the sample linear attenuation coefficient and \bar{x}_s – the average distance traveled by the photon inside the sample material which can be given as

$$\bar{x}_s = \frac{\int_{\Omega} x(\theta, \varphi) d\Omega}{\int_{\Omega} d\Omega} = \frac{\int_{\Omega} x(\theta, \varphi) \sin \theta d\theta d\varphi}{\int_{\Omega} \sin \theta d\theta d\varphi} \tag{10}$$

where θ and φ , are the polar and azimuthal angles, respectively, defining the direction of the incidence photons, while Ω is the geometrical solid angle subtended between the source and the detector and can be given by

$$\Omega = \int_{\phi} \int_{\theta} \sin \theta d\theta d\phi \tag{11}$$

Considering that $x(\theta, \varphi)$ is the possible path length traveled by the photon within the sample material with radius R_s and height L_s , using an isotropic radiating axial point source located at a distance h , from the surface of the vial, as shown in fig. 1, this can be given as

$$x_1 = \frac{L_s}{\cos \theta} \text{ and } x_2 = \frac{R_s}{\sin \theta} + \frac{h}{\cos \theta} \tag{12}$$

There are several cases to be considered in order to calculate these effective solid angles, taking into consideration the polar angle θ of the detector with a radius R_d , and height L_d , where an isotropic radiating axial point source was used and located at a distance H , from the surface of the detector crystal in the presence of a vial (filled with sample or empty) on the detector surface and in between the source and the detector.

(1) The case in which $\theta_2 > \theta_1 > \theta_4 > \theta_3$, as shown in fig. 1(a), the effective solid angles are given by

$$\Omega_{\text{Eff2}} = 2\pi \sum_{i=1}^n \Omega_i \tag{13}$$

where

$$\begin{aligned} \Omega_1 &= S_{f_1} \int_0^{\theta_3} f_{\text{att}} f_1 \sin \theta d\theta, & \Omega_2 &= S_{f_2} \int_{\theta_3}^{\theta_4} f_{\text{att}} f_1 \sin \theta d\theta \\ \Omega_3 &= \int_{\theta_4}^{\theta_1} f_{\text{att}} f_1 \sin \theta d\theta, & \Omega_4 &= \int_{\theta_1}^{\theta_2} f_{\text{att}} f_2 \sin \theta d\theta \end{aligned} \tag{14}$$

where, the self-absorption factors S_f , given in eq. (14), are expressed as

$$\begin{aligned} S_{f_1} &= e^{-\int_0^{\theta_3} \mu_s x_1 \sin \theta d\theta} e^{-\int_0^{\theta_3} \mu_d \sin \theta d\theta} \\ S_{f_2} &= e^{-\int_{\theta_3}^{\theta_4} \mu_s x_2 \sin \theta d\theta} e^{-\int_{\theta_3}^{\theta_4} \mu_d \sin \theta d\theta} \end{aligned} \tag{15}$$

The attenuation factor f_{att} , is due to the dead layer, end-cap, the absorber between the source and the detector and the side and bottom of the sample container material, described for the absorber layers with attenuation coefficients $\mu_1, \mu_2, \dots, \mu_n$, and relevant thicknesses t_1, t_2, \dots, t_n , between the source-detector system and given by

$$f_{\text{att}} = e^{-\sum_{i=1}^n \mu_i \delta_i} \tag{16}$$

with

$$\delta_i = \frac{t_i}{\cos \theta} \text{ [front absorber layers]}$$

and

$$\delta_i = \frac{t_i}{\sin \theta} \text{ [side absorber layers]}$$

where, θ_1 up to θ_4 are the extreme values of the polar angles based on the source-to-detector configuration, as shown in fig. 1, and given by

$$\begin{aligned} \theta_1 &= \tan^{-1} \frac{R_d}{H - L_d}, & \theta_2 &= \tan^{-1} \frac{R_d}{H} \\ \theta_3 &= \tan^{-1} \frac{R_s}{h - L_s}, & \theta_4 &= \tan^{-1} \frac{R_s}{h} \end{aligned} \tag{17}$$

The striking photon may enter the upper face of the detector and emerge from its base or side based on previous extreme values of the polar angles, as shown in fig. 1. These distances covered by the photon in the two cases presented can be given as

$$d_1 = \frac{L_d}{\cos \theta} \text{ and } d_2 = \frac{R_d}{\sin \theta} + \frac{H}{\cos \theta} \tag{18}$$

where $f_i = (1 - e^{-\mu_d d_i})$ and d_i are the possible path lengths traveled by the photon within the detector's active volumes d_1 and d_2 , as discussed before. While μ_d , is the total attenuation coefficient of the detector material at γ -ray energy E , where the coherent scattering part was excluded. In this and all other cases as well, the effective solid angle Ω_{Eff1} will be given by neglecting the effect of the self-absorption factor S_f .

(2) In the case in which $\theta_2 > \theta_4 > \theta_3 > \theta_1$, as shown in fig. 1(b), the effective solid angles are given by

$$\Omega_{\text{Eff2}} = 2\pi \sum_{i=1}^n \Omega_i \tag{19}$$

where

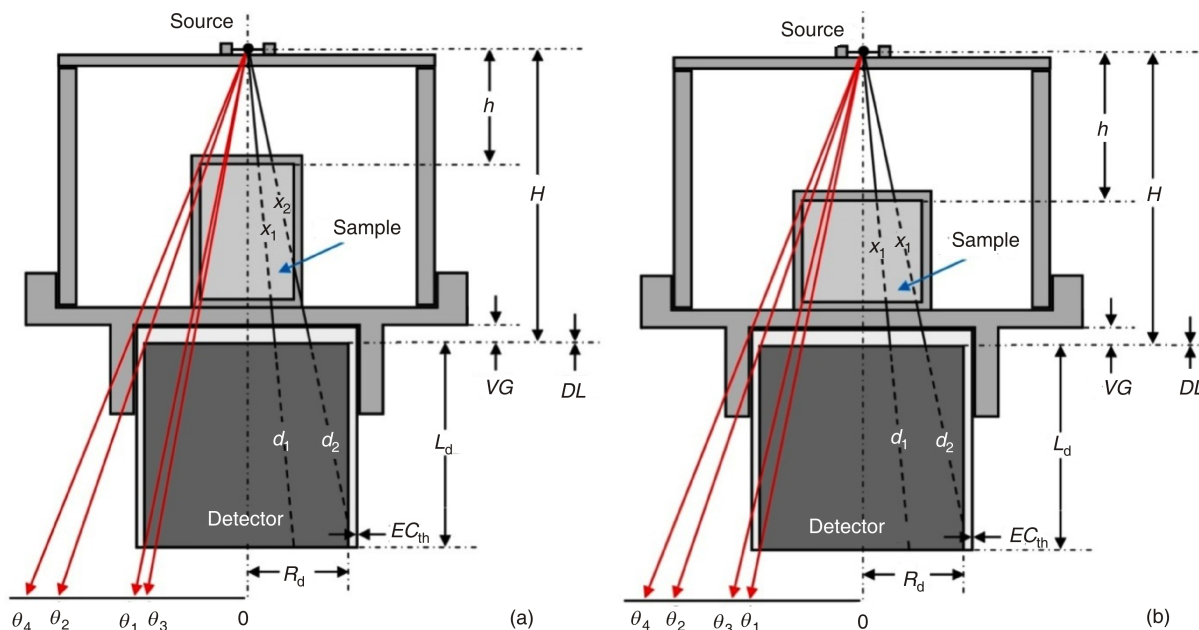


Figure 3. The geometry of the sample in arrangement between source-to-detector; (a) in case $\theta_4 > \theta_2 > \theta_1 > \theta_3$ (b) in case $\theta_4 > \theta_2 > \theta_3 > \theta_1$

$$\begin{aligned} \Omega_1 &= S_{f_1} \int_0^{\theta_1} f_{att} f_1 \sin \theta d\theta, & \Omega_2 &= S_{f_2} \int_0^{\theta_3} f_{att} f_2 \sin \theta d\theta \\ \Omega_3 &= S_{f_3} \int_{\theta_3}^{\theta_4} f_{att} f_2 \sin \theta d\theta, & \Omega_4 &= S_{f_4} \int_{\theta_4}^{\theta_1} f_{att} f_2 \sin \theta d\theta \end{aligned} \quad (20)$$

where the self absorption factors S_{f_i} , given in eq. (20) can be defined as

$$\begin{aligned} S_{f_1} &= e^{-\mu_s \int_0^{\theta_1} x_1 \sin \theta d\theta / \int_0^{\theta_1} \sin \theta d\theta} \\ S_{f_2} &= e^{-\mu_s \int_{\theta_3}^{\theta_4} x_1 \sin \theta d\theta / \int_{\theta_3}^{\theta_4} \sin \theta d\theta} \\ S_{f_3} &= e^{-\mu_s \int_{\theta_3}^{\theta_4} x_2 \sin \theta d\theta / \int_{\theta_3}^{\theta_4} \sin \theta d\theta} \end{aligned} \quad (21)$$

(3) In the case in which $\theta_2 > \theta_4 > \theta_1 > \theta_3$, as shown in fig. 2(a), the effective solid angles are given by

$$\Omega_{Eff2} = 2\pi \sum_{i=1}^n \Omega_i \quad (22)$$

where

$$\begin{aligned} \Omega_1 &= S_{f_1} \int_0^{\theta_3} f_{att} f_1 \sin \theta d\theta, & \Omega_2 &= S_{f_2} \int_0^{\theta_1} f_{att} f_1 \sin \theta d\theta \\ \Omega_3 &= S_{f_3} \int_{\theta_1}^{\theta_2} f_{att} f_2 \sin \theta d\theta, & \Omega_4 &= S_{f_4} \int_{\theta_2}^{\theta_4} f_{att} f_2 \sin \theta d\theta \end{aligned} \quad (23)$$

where the self-absorption factors S_{f_i} , given in eq. (23) can be defined as

$$\begin{aligned} S_{f_1} &= e^{-\mu_s \int_0^{\theta_3} x_1 \sin \theta d\theta / \int_0^{\theta_3} \sin \theta d\theta} \\ S_{f_2} &= e^{-\mu_s \int_{\theta_1}^{\theta_2} x_2 \sin \theta d\theta / \int_{\theta_1}^{\theta_2} \sin \theta d\theta} \\ S_{f_3} &= e^{-\mu_s \int_{\theta_2}^{\theta_4} x_2 \sin \theta d\theta / \int_{\theta_2}^{\theta_4} \sin \theta d\theta} \end{aligned} \quad (24)$$

(4) In the case in which $\theta_4 > \theta_3 > \theta_2 > \theta_1$, as shown in fig. 2(b), the effective solid angles are given by

$$\Omega_{Eff2} = 2\pi \sum_{i=1}^n \Omega_i \quad (25)$$

where

$$\begin{aligned} \Omega_1 &= S_{f_1} \int_0^{\theta_1} f_{att} f_1 \sin \theta d\theta, \\ \Omega_2 &= S_{f_2} \int_{\theta_1}^{\theta_2} f_{att} f_2 \sin \theta d\theta \end{aligned} \quad (26)$$

where the self absorption factors S_{f_i} , given in eq. (26) can be expressed as

$$\begin{aligned} S_{f_1} &= e^{-\mu_s \int_0^{\theta_1} x_1 \sin \theta d\theta / \int_0^{\theta_1} \sin \theta d\theta} \\ S_{f_2} &= e^{-\mu_s \int_{\theta_1}^{\theta_2} x_1 \sin \theta d\theta / \int_{\theta_1}^{\theta_2} \sin \theta d\theta} \end{aligned} \quad (27)$$

(5) In the case in which $\theta_4 > \theta_2 > \theta_1 > \theta_3$, as shown in fig. 3(a), the effective solid angles are given by

$$\Omega_{Eff2} = 2\pi \sum_{i=1}^n \Omega_i \quad (28)$$

where

$$\begin{aligned} \Omega_1 & S_{f_1} \int_{\theta_1}^{\theta_3} f_{att} f_1 \sin \theta d\theta \\ \Omega_2 & S_{f_2} \int_{\theta_2}^{\theta_3} f_{att} f_1 \sin \theta d\theta \\ \Omega_3 & S_{f_3} \int_{\theta_1}^{\theta_2} f_{att} f_2 \sin \theta d\theta \end{aligned} \quad (29)$$

where the self-absorption factors S_f , given in eq. (29) can be defined as

$$\begin{aligned} S_{f_1} &= e^{-\mu_s \int_{\theta_1}^{\theta_3} x_1 \sin \theta d\theta / \int_{\theta_1}^{\theta_3} \sin \theta d\theta} \\ S_{f_2} &= e^{-\mu_s \int_{\theta_2}^{\theta_3} x_2 \sin \theta d\theta / \int_{\theta_2}^{\theta_3} \sin \theta d\theta} \\ S_{f_3} &= e^{-\mu_s \int_{\theta_1}^{\theta_2} x_2 \sin \theta d\theta / \int_{\theta_1}^{\theta_2} \sin \theta d\theta} \end{aligned} \quad (30)$$

(6) In the case in which $\theta_4 > \theta_2 > \theta_3 > \theta_1$, as shown in fig. 3(b), the effective solid angles are given by

$$\Omega_{Eff2} = 2\pi \sum_{i=1}^n \Omega_i \quad (31)$$

where

$$\begin{aligned} \Omega_1 & S_{f_1} \int_{\theta_1}^{\theta_3} f_{att} f_1 \sin \theta d\theta \\ \Omega_2 & S_{f_2} \int_{\theta_2}^{\theta_3} f_{att} f_2 \sin \theta d\theta \\ \Omega_3 & S_{f_3} \int_{\theta_1}^{\theta_2} f_{att} f_2 \sin \theta d\theta \end{aligned} \quad (32)$$

where the self-absorption factors S_f , given in eq. (32) can be defined as

$$\begin{aligned} S_{f_1} &= e^{-\mu_s \int_{\theta_1}^{\theta_3} x_1 \sin \theta d\theta / \int_{\theta_1}^{\theta_3} \sin \theta d\theta} \\ S_{f_2} &= e^{-\mu_s \int_{\theta_2}^{\theta_3} x_1 \sin \theta d\theta / \int_{\theta_2}^{\theta_3} \sin \theta d\theta} \\ S_{f_3} &= e^{-\mu_s \int_{\theta_1}^{\theta_2} x_2 \sin \theta d\theta / \int_{\theta_1}^{\theta_2} \sin \theta d\theta} \end{aligned} \quad (33)$$

Finally, the formulae of the self absorption factors S_f can be rewritten and given by the next equation based on eqs. (4) and (9), and all of the above discussions for each case

$$S_f = e^{-\mu_s \sum_{i=1}^n \bar{x}_i} \quad (34)$$

where the factor i , refers to the average possible path lengths traveled by the photon within the sample volume, depending on the position of the incidence photon. The average path lengths in eq. (34) pass through the sample material and, by using the available ratio from eq. (4), it is possible to calculate the linear attenuation coefficient of any sample material.

EXPERIMENTAL MATERIALS AND METHODS

A coaxial HPGe Canberra spectrometer, model GC1520, with a volume of approximately 100 cm³ and energy range of 40 keV to >10 MeV, was used to detect the gamma rays. The detector's cold finger was placed in a cryostat, model 7500SL. The main technical features provided by the manufacturer: diameter and length of the crystal of 48 mm and 54.5 mm, respectively. In addition, as shown in fig. 1, the end-cap to the crystal distance, VG, was 5 mm, the entrance window, EC_{th}, was 1.5 mm of Al and the dead layer, DL, was 0.5 mm of Ge. The relative efficiency of the detector was 15 % and the resolution (FWHM) at 1.33 MeV of ⁶⁰Co was 1.85 keV. Standard electronics, such as a built-in pre-amplifier model 2002CSL, HV power supply, model 3106D, providing (+)4500 Vdc recommended as the bias voltage, an amplifier (model 2026) with a time constant of 4 μs and a 8 k computerized multi-channel analyzer, were coupled with the detector system. The detector was kept in a 15 cm thick lead castle to attenuate cosmic and environmental radiation, with a copper lining on the inside to absorb any lead X-rays that are produced. In order to eliminate low background noise, the lower level discriminator (LLD) was adjusted at 1 % of its maximum limit. Fine gain and gain were adjusted to get well-defined gamma-ray spectra. The spectra were recorded and processed by the Genie 2000 data acquisition and analysis software made by Canberra.

The energy of incident gamma radiation used in the study was varied by using five gamma emitting point sources: ²⁴¹Am (59.52 keV), ¹³³Ba (80.99 keV), ¹⁵²Eu (121.78, 244.69, 344.28, 778.90, 964.13, and 1408.01 keV), ¹³⁷Cs (661.66 keV) and ⁶⁰Co (1173.23 and 1332.50 keV). The activity of the previous sources (June 1st, 2009), was in kBq (259.0 ± 2.6, 275.3 ± 2.8, 290.0 ± 4.0, 285.0 ± 4.0, and 212.1 ± 1.5, respectively). The point sources used were purchased from the Physikalisch-Technische Bundesanstalt (PTB), Braunschweig and Berlin, the highest German technical authority in the field of metrology and certain sectors of safety engineering. The radioactive material was a very slight round deposit, about 5 mm in diameter, placed in the middle of two polyethylene foils, each having a mass per unit area of (21.3

1.8) mg/cm². Under pressure and by heating, the two foils were welded and sealed along the length of the area and, thus, rendered leakproof. To enable handling, a 26 mm-diameter foil was mounted onto a circular aluminum ring (external diameter: 30 mm, height: 3 mm) from which it could easily be removed, if and when necessary.

All measured spectra were recorded from the above mentioned sources, which, measured by using a special Plexiglas holder, offer a broad and free solid angle between the source and the detector, as shown in

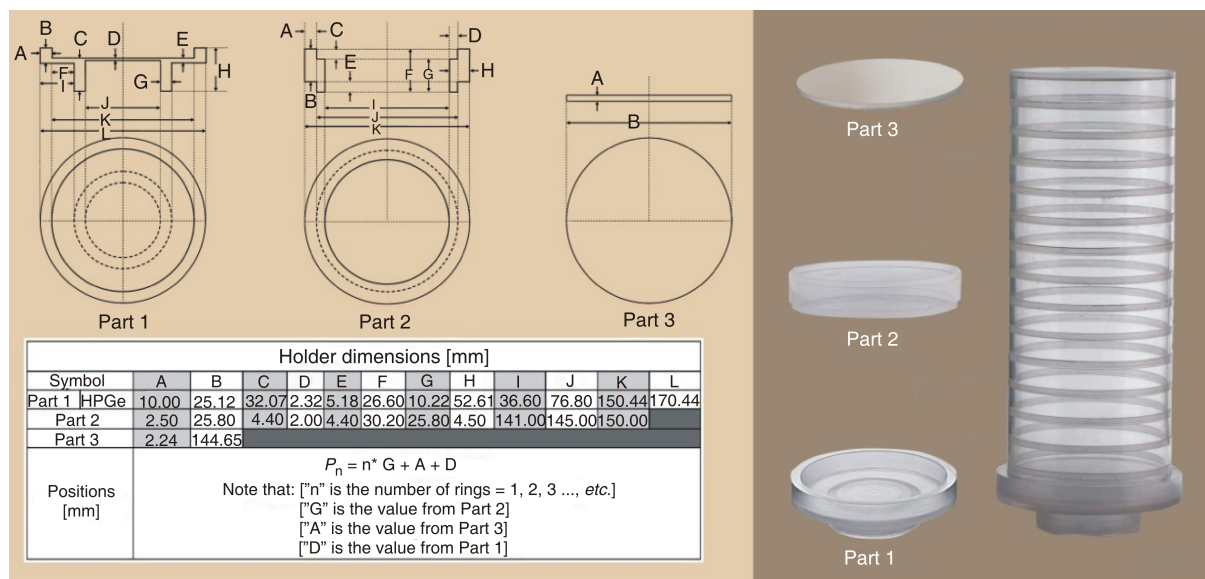


Figure 4. Geometrical drawing of the different parts of the homemade Plexiglas holder

Figure 5. Geometrical drawing of the empty homemade Plexiglas vial

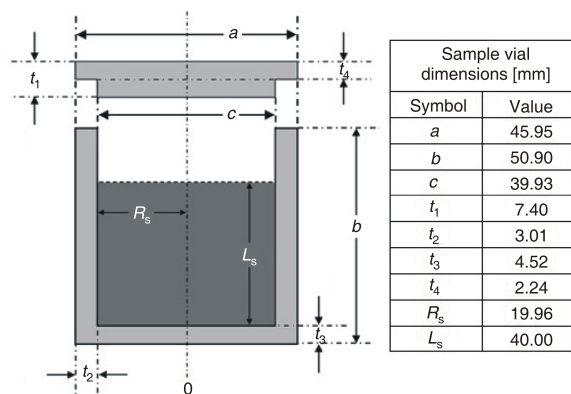


fig. (4). The holder has a thick enough base placed straightforwardly onto the detector entrance window as an absorber, so as to avoid the effect of β^- and X-rays and protect the detector heads. It also excludes the need for the correction of X-gamma coincidences since, in most cases, the associating X-rays are sufficiently weak to be completely absorbed before entering the detector. In order to prevent dead time, pile-up and coincidence summing effects, a large source-to-detector axial distance was considered from the detector endcap. As for measurement geometry, sources were kept at a fixed distance of 26.40 cm from the detector endcap.

A homemade Plexiglas vial, of a density of 1.19 g/cm^3 , was axially introduced in-between the detector and the radioactive point source inside the holder house and kept on the top of the holder base. Measurements were done in both the empty and the full vial, as well as the ones filled with various samples of NaCl, Na_2CO_3 , and $(\text{NH}_4)_2\text{SO}_4$ with densities uniformly approximated at 1.39, 1.30, and 1.16 g/cm^3 , respectively, which are similar to the densities of the environmental samples and allow for the large self-attenuation effect in the low and medium energy

region, as well. The geometrical drawing of the vial was given as shown in fig. (5), where the height of each sample inside the vial was fixed and kept at exactly 4 cm.

As to insure adequate quality of calibration and measurement, a detector with a minimum of electronics noise and unwanted pulses must be taken into consideration. Experimental measurements of both processes were done via a good stabilizer and a good system configuration separating it from the walls and floors of the room. The calibration of the multi-channel analyzer converts the channel number relative to the signal amplitude into incident gamma ray energy. Prior to the measurement procedures, the detector was calibrated by using three radioactive sources: ^{241}Am (59.52 keV), ^{137}Cs (661.66 keV) and ^{60}Co (1173.23 and 1332.50 keV) to approximately cover the entire energy range of measurements.

Data acquisition and spectrum control were done by PC through a USB port based on acquisition and analysis software (ISO 9001, Genie 2000). The acquisition time was as long as required to get high and sufficiently numerous counts under each peak of interest with a statistical uncertainty less than 1 %. The

peak fitting was performed via a Gaussian shape without the germanium low-energy tail.

Spectrum analysis is the main task of Genie 2000. Before the analysis itself, a choice of peak regions is required. This was done by selecting the region of interest (ROI) situated between the start and the end of the desired channels. Each full-energy peak of the recorded spectrum was identified, the ROI fixed, background subtracted under each peak and then, finally, the count rate under the wanted peak recorded, whether the vial was empty or filled with the sample under investigation. The measured count rates were used to estimate the linear attenuation coefficient of each sample, based on the specified energy range of gamma ray sources.

RESULTS AND DISCUSSION

In the previous section, an explanation was given for measurement of the self-absorption factor and linear attenuation coefficient of different sample materials by means of an experimental technique. In this section, a broad comparison between these values and those expected in theory will be made in order to check the reliability of the present method in which the values acquired by both methods are based on the calculated average path distance traveled by the photon inside the sample materials. The variation of the calculated self-attenuation factor, S_f , of the various samples of NaCl, Na_2CO_3 , and $(\text{NH}_4)_2\text{SO}_4$ and their densities as a function of photon energy can be given as in fig. (6). These values were obtained based on the ratio of the effective solid angle in eq. (4) and according to an online database of the reference linear attenuation coefficient [20].

The variation of the calculated linear attenuation coefficient, μ_s , of the same samples as a function of their density and photon energy can also be given as in fig. (7). They were estimated based on the previous values of the calculated self-attenuation factor, S_f and the average path distance traveled by the photon inside the sample materials, as shown in eq. 10. Our mathematical model takes into account integration limitations of case (2.6) regarding the differences in the physical and chemical properties of the samples stored in a relatively large Plexiglas vial in order to be representative enough of the self-attenuation correction factor.

Table 1 shows the calculated values of the self-attenuation factor S_f , compared with the ones measured, obtained from the ratio in eq. (4) between the measured gamma ray count rates in a vial filled with sample materials and an empty vial, respectively. Furthermore, the same table contains a comparison between the online database of the reference (XCOM), the calculated and the measured linear attenuation coefficient, where the measured values of the linear attenuation coefficient were determined depending on the ratio of the measured count rates of gamma rays in eq. (4) and the average path distance in

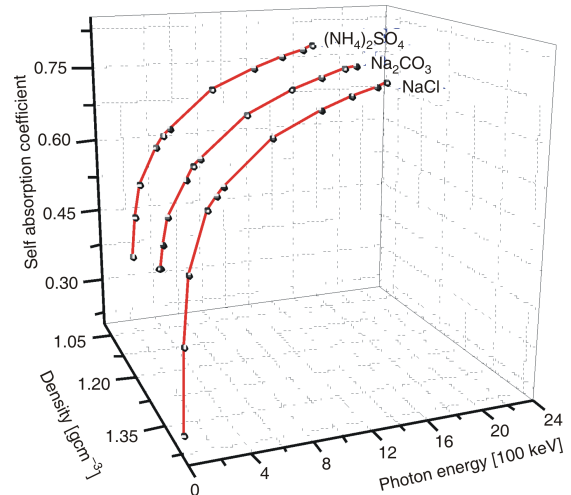


Figure 6. The variation of the calculated self-attenuation factor of the various samples of NaCl, Na_2CO_3 , and $(\text{NH}_4)_2\text{SO}_4$ and their densities as a function of photon energy

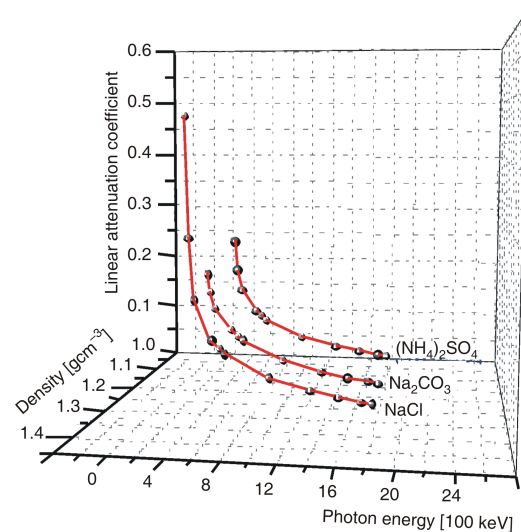


Figure 7. The variation of the calculated linear attenuation coefficient of the various samples of NaCl, Na_2CO_3 , and $(\text{NH}_4)_2\text{SO}_4$ and their densities as a function of photon energy

eq. (10) traveled by the photon inside the sample materials. The deviation percentage between the XCOM and the measured linear attenuation coefficient values is Δ_1 . Also, Δ_2 is the deviation percentage between the XCOM and the calculated linear attenuation coefficient values, while Δ_3 is the deviation percentage between the measured and the calculated self-attenuation factor based on the following equations, respectively,

$$\begin{aligned} \Delta_1 &= \frac{\mu_{\text{measured}} - \mu_{\text{XCOM}}}{\mu_{\text{measured}}} 100 [\%] \\ \Delta_2 &= \frac{\mu_{\text{calculated}} - \mu_{\text{XCOM}}}{\mu_{\text{calculated}}} 100 [\%] \\ \Delta_3 &= \frac{S_f(\text{calculated}) - S_f(\text{measured})}{S_f(\text{calculated})} 100 [\%] \end{aligned} \quad (35)$$

Table 1. The variation of the linear attenuation coefficient μ and the self-attenuation factor S_f , including its deviation percentage

Sample name	Energy [keV]	μ [cm^{-1}]			S_f		Deviation percentage		
		XCOM	Measured	Calculated	Measured	Calculated	Δ_1 [%]	Δ_2 [%]	Δ_3 [%]
NaCl	59.53	4.447E-01	4.647E-01	4.676E-01	2.108E-01	2.088E-01	4.30	4.90	-0.97
	80.99	2.886E-01	2.847E-01	2.986E-01	3.853E-01	3.678E-01	-1.37	3.35	-4.76
	121.78	2.091E-01	2.077E-01	2.111E-01	4.987E-01	4.930E-01	-0.67	0.94	-1.15
	244.69	1.547E-01	1.574E-01	1.536E-01	5.903E-01	5.977E-01	1.72	-0.69	1.23
	302.85	1.422E-01	1.453E-01	1.430E-01	6.145E-01	6.193E-01	2.13	0.59	0.77
	344.28	1.354E-01	1.319E-01	1.346E-01	6.429E-01	6.370E-01	-2.65	-0.57	-0.93
	661.66	1.032E-01	1.011E-01	1.033E-01	7.126E-01	7.074E-01	-2.08	0.14	-0.74
	964.13	8.657E-02	8.822E-02	8.608E-02	7.441E-01	7.495E-01	1.87	-0.57	0.72
	1173.23	7.848E-02	7.995E-02	7.924E-02	7.650E-01	7.668E-01	1.84	0.97	0.24
	1332.50	7.360E-02	7.383E-02	7.397E-02	7.809E-01	7.805E-01	0.31	0.49	-0.05
1408.01	7.165E-02	7.000E-02	7.126E-02	7.910E-01	7.876E-01	-2.36	-0.55	-0.43	
Na ₂ CO ₃	59.53	2.410E-01	2.334E-01	2.298E-01	4.575E-01	4.630E-01	-3.26	-4.86	1.19
	80.99	2.110E-01	2.066E-01	2.025E-01	5.005E-01	5.074E-01	-2.13	-4.19	1.36
	121.78	1.810E-01	1.837E-01	1.758E-01	5.403E-01	5.550E-01	1.47	-2.97	2.64
	244.69	1.460E-01	1.450E-01	1.435E-01	6.153E-01	6.183E-01	-0.69	-1.73	0.49
	302.85	1.360E-01	1.320E-01	1.349E-01	6.425E-01	6.364E-01	-3.03	-0.80	-0.97
	344.28	1.290E-01	1.252E-01	1.272E-01	6.573E-01	6.531E-01	-3.04	-1.45	-0.64
	661.66	9.325E-02	9.186E-02	9.513E-02	7.351E-01	7.271E-01	-1.51	1.97	-1.10
	964.13	7.808E-02	7.846E-02	7.881E-02	7.689E-01	7.680E-01	0.48	0.92	-0.12
	1173.23	7.069E-02	7.066E-02	7.237E-02	7.892E-01	7.847E-01	-0.04	2.32	-0.57
	1332.50	6.641E-02	6.739E-02	6.728E-02	7.979E-01	7.982E-01	1.45	1.30	0.04
1408.01	6.459E-02	6.602E-02	6.435E-02	8.016E-01	8.061E-01	2.17	-0.37	0.55	
(NH ₄) ₂ SO ₄	59.53	2.650E-01	2.760E-01	2.614E-01	3.967E-01	4.165E-01	3.99	-1.36	4.76
	80.99	2.117E-01	2.071E-01	2.084E-01	4.997E-01	4.975E-01	-2.22	-1.59	-0.44
	121.78	1.782E-01	1.826E-01	1.726E-01	5.425E-01	5.609E-01	2.41	-3.24	3.28
	244.69	1.400E-01	1.379E-01	1.403E-01	6.301E-01	6.250E-01	-1.52	0.23	-0.82
	302.85	1.296E-01	1.309E-01	1.302E-01	6.450E-01	6.465E-01	0.99	0.48	0.23
	344.28	1.238E-01	1.287E-01	1.217E-01	6.497E-01	6.651E-01	3.81	-1.71	2.32
	661.66	9.453E-02	9.648E-02	9.497E-02	7.238E-01	7.275E-01	2.02	0.46	0.51
	964.13	7.937E-02	7.820E-02	7.809E-02	7.695E-01	7.698E-01	-1.50	-1.63	0.04
	1173.23	7.208E-02	7.070E-02	7.257E-02	7.891E-01	7.842E-01	-1.95	0.68	-0.63
	1332.50	6.757E-02	6.656E-02	6.711E-02	8.001E-01	7.986E-01	-1.52	-0.68	-0.18
1408.01	6.560E-02	6.577E-02	6.572E-02	8.022E-01	8.024E-01	0.26	0.18	0.02	

From figs. (6) and (7) in tab. (1), it is evident that: self-attenuation factors are of utmost importance, especially in the low and medium energy region, because when the self-attenuation factor is not present in the calculations, this causes an increase in full-energy peak efficiency values and will act as the main source of uncertainty in volume measurement. Underestimation of the measured activity is also a possibility if the reference efficiency values are measured by using a standard source of the water matrix and the densities of the measured samples differ considerably from that of the source. The self-attenuation factor increases rapidly with the decrease of energy in different materials and reaches high values based on the density, material composition and the heightened probability of the photon traveling distances within the source matrix itself.

The linear attenuation coefficient for the various photon interaction processes is high at the start and then decreases sharply with a rise in photon energy up to 100 keV for all selected composite materials, due to the dominance of the three main incident photon pro-

cesses. The values of the calculated and measured linear attenuation coefficients are in close agreement with the reference linear attenuation coefficient from the online database (XCOM) used to calculate deviation percentage values.

This study was designed and based on simplified devices without a collimator to verify the mathematical model by using reference sample materials to calculate the linear attenuation coefficient. Nevertheless, it can be widely applied if vial samples in different geometries and shapes, discussed in *Mathematical model*, are present in cited mathematical calculations, allowing easy determination for the self-attenuation factor of all sample types.

CONCLUSION

In this work, a novel straightforward method based on source-to-detector geometry and configuration and the calculation of the average path length dis-

tance traveled by the photon inside the sample materials was used to determine the linear attenuation coefficient. The same method was used to correct the self-attenuation effect inside the environmental volumetric samples. The value of full-energy peak efficiency of the volumetric samples depends on the composition and densities of the samples. Deviation percentages show a 5 % level of efficiency of the method. The method could, thus, serve as an effective and inexpensive tool to be used by inexpert technicians in routine measurements of gamma ray spectrometry involving homogenous and unfamiliar samples.

ACKNOWLEDGMENT

The author is indebted to Prof. Dr. M. I. Abbas for his fruitful suggestions and contribution.

REFERENCES

- [1] Robu, E., Giovani, C., Gamma-Ray Self-Attenuation Corrections in Environmental Samples, *Rom. Rep. Phys.*, 61 (2009), 2, pp. 295-300
- [2] Miguela, S., *et al.*, A Semi-Empirical Approach for Determination of Low-Energy Gamma-Emitters in Sediment Samples with Coaxial Ge-Detectors, *Appl. Radiat. Isot.*, 61 (2004), 2-3, pp. 361-366
- [3] Abbas, M. I., HPGe Detector Photopeak Efficiency Calculation Including Self-Absorption and Coincidence Corrections for Cylindrical Sources Using Compact Analytical Expressions, *Radiat. Phys. Chem.*, 61 (2001), 3-6, pp. 429-431
- [4] Hernandez, F., El-Daoushy, F., Semi-Empirical Method for Self-Absorption Correction of Photons with Energies as Low as 10 keV in Environmental Samples, *Nucl. Instrum. Meth.*, 484 (2002), 1-3, pp. 625-641
- [5] Berger, M., *et al.*, XCOM: Photon Cross Sections Database, NBSIR 87-3597. NIST, PML, Radiation and Biomolecular Physics Division, 2010
- [6] Colgate, S. A., Gamma-Ray Absorption Measurements, *Phys. Rev.*, 87 (1952), 4, pp. 592-601
- [7] Wiedenbeck, M., Total X-Ray Attenuation Coefficients from 40 keV to 412 keV, *Phys. Rev.*, 126 (1962), 3, pp. 1009-1010
- [8] Conner, A. L., Gamma-Ray Attenuation-Coefficient Measurements, *Phys. Rev. A.*, 1 (1970), 3, pp. 539-544
- [9] Kim, C. J., *et al.*, Mathematical Approach to Determine the Linear Attenuation Coefficient without Collimator in Gamma-Ray Spectrometry, *Radiat. Prot. Dosi*, 155 (2013), 2, pp. 236-240
- [10] Nakamura, T., Suzuki, T., Monte Carlo Calculation of Peak Efficiencies of Ge(Li) and Pure Ge Detectors to Voluminal Sources and Comparison with Environmental Radioactivity Measurement, *Nucl. Instrum. Meth.*, 205 (1983), 1-2, pp. 211-218
- [11] Mortreau, P., Berndt, R., Attenuation of a Non-Parallel Beam of Gamma Radiation by Thick Shielding-Application to the Determination of the ²³⁵U Enrichment with NaI Detectors, *Nucl. Instrum. Meth.*, 550 (2005), 3, pp. 675-690
- [12] Gupta, S., Gurdeep, S., Gamma-Rays Absorption Studies of Garnet Series of Gemstones at 1 keV to 100 GeV: Theoretical Calculation, *Journal of Engineering (IOSRJEN)*, 4 (2014), 2, pp. 01-08
- [13] Sima, O., Dovlete, C., Matrix Effects in the Activity Measurement of Environmental Samples-Implementation of Specific Corrections in a Gamma-Ray Spectrometry Analysis Program, *Appl. Radiat. Isot.*, 48 (1997), 1, pp. 59-69
- [14] Sima, O., *et al.*, GESPECOR – A Versatile Tool in Gamma-Ray Spectrometry, *Journal of Radioanalytical Nuclear Chemistry*, 248 (2001), 2, pp. 359-364
- [15] Hubbell, J., Photon Mass Attenuation and Energy-Absorption Coefficients, *Appl. Radiat. Isot.*, 33 (1982), pp. 1269-1290
- [16] Abbas, M. I., Direct Mathematical Method for Calculating Full-Energy Peak Efficiency and Coincidence Corrections of HPGe Detectors for Extended Sources, *Nucl. Instrum. Meth.*, 256 (2007), 1, pp. 554-557
- [17] Abbas, M. I., A New Analytical Method to Calibrate Cylindrical Phoswich and LaBr₃(Ce) Scintillation Detectors, *Nucl. Instrum. Meth.*, 621 (2010), 1-3, pp. 413-418
- [18] Thabet, A. A., *et al.*, Experimental Verification of Gamma-Efficiency Calculations For Scintillation Detectors in Angle 4 Software, *Nucl Technol Radiat*, 30 (2015), 1, pp. 35-46
- [19] Badawi, M. S., *et al.*, A Numerical Approach to Calculate the Full-Energy Peak Efficiency of HPGe Well-Type Detectors Using the Effective Solid Angle Ratio, *Journal of Instrumentation*, 9 (2014), 7, P07030
- [20] ***, XCOM Photon Cross-Sections Database, National Institute of Standards and Technology, Physical Measurements Laboratory, <http://physics.nist.gov/PhysRefData/Xcom/html/xcom1.html>.

Received on September 7, 2015

Accepted on November 20, 2015

Мохамед С. БАДАВИ

**МЕТОДА НУМЕРИЧКЕ СИМУЛАЦИЈЕ ЗА ПРОРАЧУН ЛИНЕАРНИХ
КОЕФИЦИЈЕНАТА СЛАБЉЕЊА НЕИДЕНТИФИКОВАНИХ МАТЕРИЈАЛА
У РУТИНСКОЈ ГАМА СПЕКТРОМЕТРИЈИ**

Када се користи гама спектрометрија за радиоактивну анализу узорка из животне средине (као што су земљиште, седимент, или пепео живог организма), потребно је познавати одговарајуће линеарне коефицијенте слабљења како би се израчунала самоапсорпција у телу узорка. Овај параметар је утолико важнији јер су неидентификовани узорци различити по саставу и густини од референтних (при чему референтни узорци могу бити течни извори, који се уобичајено користе за калибрацију ефикасности детекције у мониторингу радиоактивности). Овај рад има за циљ да уведе нумеричку симулациону методу за прорачун линеарних коефицијената слабљења без примене колиматора. Метода је пре свега заснована на прорачунима ефективних просторних углова – параметара једињења који одређују вероватноће емисије и детекције, као и за геометријску конфигурацију извор-детектора. Такође су примењени принцип трансфера ефикасности и средњих дужина слободног пута кроз узорке. Добијени резултати упоређени су са NIST-XCOM базама података и блиско слагање резултата потврђује оправданост нумеричке симулационе методе.

Кључне речи: гама спектрометрија, линеарни коефицијент слабљења, ефективан просторни угао, средња дужина слободног пута, нумеричка симулациона метода
